frontiers in Marine Science

ORIGINAL RESEARCH
published: 23 December 2021
doi: 10.3389/fmars.2021.725713

Dissolved Nitrous Oxide and Hydroxylamine in the South Yellow Sea and the East China Sea During Early Spring: Distribution, Production, and Emissions

*Xueji Gu[1,2], Fang Cheng[1,2], Xiaolei Chen[1,2], Guanxiang Du[1,2] and Guiling Zhang[1,2]**

[1] Frontiers Science Center for Deep Ocean Multispheres and Earth System, Key Laboratory of Marine Chemistry Theory and Technology, Ministry of Education, Ocean University of China, Qingdao, China, [2] Laboratory for Marine Ecology and Environmental Science, Qingdao National Laboratory for Marine Science and Technology, Qingdao, China

Coastal marine systems are active regions for the production and emission of nitrous oxide (N_2O), a potent greenhouse gas. Due to the inherently high variability in different coastal biogeochemical cycles, the factors and mechanisms regulating coastal N_2O cycling remain poorly understood. Hydroxylamine (NH_2OH), a potential precursor of N_2O, has received less attention than other compounds in the coastal areas. Here, we present the spatial distribution of N_2O and the first reported NH_2OH distribution in the South Yellow Sea (SYS) and the East China Sea (ECS) between March and April 2017. The surface N_2O concentrations in the SYS and the ECS varied from 5.9 to 11.3 nmol L^{-1} (average of 8.4 ± 1.4 nmol L^{-1}) and were characterized by offshore and north–south decreasing gradients. NH_2OH showed patchy characteristics and was highly variable, fluctuating between undetectable to 16.4 nmol L^{-1}. We found no apparent covariation between N_2O and NH_2OH, suggesting the NH_2OH pathway, i.e., nitrification (ammonium oxidation), was not the only process affecting N_2O production here. The high NH_2OH values co-occurred with the greatest chlorophyll-*a* and oxygen levels in the nearshore region, along with the relationships between NO_2^-, NO_3^-, and NH_2OH, indicating that a "fresh" nitrifying system, favoring the production and accumulation of NH_2OH, was established during the phytoplankton bloom. The high N_2O concentrations were not observed in the nearshore. Based on the correlations of the excess N_2O (ΔN_2O) and apparent oxygen utilization, as well as ΔN_2O vs. NO_3^-, we concluded that the N_2O on the continental shelf was mainly derived from nitrification and nitrifier denitrification. Sea-to-air fluxes of N_2O varied from −12.4 to 6.6 μmol m^{-2} d^{-1} (−3.8 ± 3.7 μmol m^{-2} d^{-1}) using the Nightingale et al. (2000) formula and −13.3 to 6.9 μmol m^{-2} d^{-1} (−3.9 ± 3.9 μmol m^{-2} d^{-1}) using the Wanninkhof (2014) formula, which corresponds to 75–112% in saturation, suggesting that the SYS and the ECS acted overall as a sink of atmospheric N_2O in early spring, with the strength weakening. Our results reveal the factors and potential mechanisms controlling the production and accumulation of NH_2OH and N_2O in the SYS and the ECS during early spring.

Keywords: nitrous oxide, hydroxylamine, nitrification, nitrifier denitrification, East China Sea, South Yellow Sea

OPEN ACCESS

Edited by:
Jeomshik Hwang,
Seoul National University,
South Korea

Reviewed by:
Liyang Zhan,
State Oceanic Administration, China
Keyhong Park,
Korea Polar Research Institute,
South Korea

****Correspondence:***
Guiling Zhang
guilingzhang@ouc.edu.cn

Specialty section:
This article was submitted to Marine Biogeochemistry, a section of the journal Frontiers in Marine Science

Received: *15 June 2021*
Accepted: *29 November 2021*
Published: *23 December 2021*

Citation:
Gu X, Cheng F, Chen X, Du G and Zhang G (2021) Dissolved Nitrous Oxide and Hydroxylamine in the South Yellow Sea and the East China Sea During Early Spring: Distribution, Production, and Emissions. Front. Mar. Sci. 8:725713. doi: 10.3389/fmars.2021.725713

INTRODUCTION

Oceans represent the second important natural source of the climatically important trace gas nitrous oxide (N_2O), a compound that plays a pivotal role in the global greenhouse effect and atmospheric chemistry generally (Stocker et al., 2013). Observations and models estimate global oceanic N_2O emissions of 2.5–4.2 Tg N yr^{-1}, which is believed to contribute about 20% of the global N_2O emissions (Buitenhuis et al., 2018; Tian et al., 2020; Yang et al., 2020). However, these estimations still suffer from large uncertainties, partly because of sparse data coverage in the highly dynamic and productive coastal oceans.

Marine N_2O production and consumption are primarily carried out by nitrifying and denitrifying microbes. In the presence of oxygen, N_2O can be produced as a byproduct of nitrification ($NH_4^+ \rightarrow NO_2^- \rightarrow NO_3^-$) by nitrifying microbes (Kuypers et al., 2018). Instead of ammonia-oxidizing bacteria (AOB), ammonia-oxidizing archaea (AOA) is responsible for ammonium oxidation during nitrification, and numerically dominant among ammonia-oxidizing organisms in large parts of the oceans (Santoro et al., 2011; Löscher et al., 2012; Martens-Habbena et al., 2015; Frame et al., 2017; Toyoda et al., 2019). However, it is still argued whether AOA could produce N_2O via ammonium oxidation similar to AOB, as no archaeal hydroxylamine oxidoreductase homolog has been found (Löscher et al., 2012; Vajrala et al., 2013; Stieglmeier et al., 2014). Under low-oxygen and suboxic conditions, N_2O production can also occur via the reduction of nitrite by AOA and AOB, referred to as nitrifier–denitrification (Santoro et al., 2011; Kozlowski et al., 2016). Also, in hypoxic and anoxic zones, N_2O is produced and consumed during the stepwise reduction of nitrate to N_2 by denitrifying organisms, depending on the bioavailable oxygen (Bange et al., 2010; Kuypers et al., 2018).

Hydroxylamine (NH_2OH), an intermediate of nitrogen cycling, is a precursor of N_2O produced via ammonium oxidation. Both AOA and AOB can produce and consume NH_2OH during the oxidation of ammonium in diverse oxygen conditions (Sutka et al., 2003; Vajrala et al., 2013). Thus, observations of temporal and spatial variabilities and controls on NH_2OH in marine environments will enable the examination of the mechanisms driving N_2O biogeochemistry, especially the NH_2OH pathway. Unlike N_2O, however, it is difficult to measure *in situ* NH_2OH concentrations because of its short living time of only a few hours in seawaters (Butler et al., 1987, 1988). Since the first reported marine observation of NH_2OH off the Oregon coast (Von Breymann et al., 1982), only a few studies have been conducted in the field of oceans. Gebhardt et al. (2004) and Schweiger et al. (2007) reported a striking seasonal pattern for NH_2OH in the Baltic Sea and found that the dramatic increase of NH_2OH was closely associated with reoxygenation conditions in the short term, and the accompanying onset of a "fresh" nitrifying system, namely, the ammonia oxidation rates exceeded that of nitrite oxidation. The first record of the positive correlation of the concentrations of N_2O and NH_2OH was a recent study of the eastern tropical South Pacific and the equatorial Atlantic Ocean from Korth et al. (2019). This revealed that NH_2OH is a potential proxy for active nitrification and *in situ* N_2O production in the open ocean.

Coastal areas, globally important transitional ecosystems, connect marine and terrestrial environments, and are highly susceptible to anthropogenic impacts. Biogeochemical cycling of coastal ecosystems is being substantially altered by excess anthropogenic nutrient inputs and the widespread increase of pollutants in diverse forms (Doney, 2010; Jurasinski et al., 2018). These anthropogenic perturbations increase uncertainty in the N_2O budget and drive variabilities in coastal zones (Wilson et al., 2020). Long-term observations in coastal areas show pronounced seasonal and interannual dynamics for N_2O patterns compared with the open ocean (Farías et al., 2015; Ma et al., 2019; Ganesan et al., 2020). The production and emissions of N_2O in the coastal zones highly exceed those in the open ocean (Frame et al., 2014; Fenwick and Tortell, 2018). Based on the projections of growing anthropogenic nitrogenous nutrient inputs, coastal N_2O emissions are widely recognized as a gradually increasing trend in the future (Bange et al., 2010). Recent observations and models, however, suggest that future N_2O emissions in coastal regions will present a decreasing trend, following the escalating regulation of anthropogenic pollution and nutrient discharge (Landolfi et al., 2017; Battaglia and Joos, 2018; Bange et al., 2019; Ma et al., 2019). Therefore, repeat observation for N_2O with regular time intervals is necessary for the coastal zones.

Since the first study of the N_2O in the northeastern East China Sea (ECS) by Zhang et al. (2008), researchers have carried out studies in the Yellow Sea (YS) (Yang et al., 2009), the East China Sea shelf (Wang et al., 2016), and the Yangtze River Estuary and its adjacent waters (Zhang et al., 2010). These studies found that disproportionately high N_2O emissions occurred in the ECS and the YS, which are only a small proportion of world ocean areas. Chen et al. (2021) reported the N_2O distribution and emissions in the ECS and the South Yellow Sea (SYS) in four seasons of 2011 and found a pronounced seasonal fluctuation with the higher fluxes in spring and summer and lower fluxes in fall and winter. Previous studies intensively focused on the distributions and budgets of N_2O in the marginal seas of China, whereas the production mechanisms have received much less attention. Besides, NH_2OH in the marginal seas of the Pacific is still not constrained.

Here, we present the N_2O and NH_2OH distributions in the SYS and the ECS in the early spring of 2017. We integrated the analyses of N_2O, NH_2OH, and a variety of active biological elements (chlorophyll-*a*, O_2, and nitrogenous nutrients) and discussed the potential *in situ* biological production processes of N_2O.

MATERIALS AND METHODS

Hydrographic Settings

Surrounded by the Chinese mainland, the Taiwan Island, the Ryukyu Islands, and the Korea Peninsula, the SYS and the ECS are the marginal seas of the western Pacific Ocean (**Figure 1A**). The SYS is a shallow and a semiclosed continental shelf sea with a surface area of 3.09×10^5 km^2 and an average depth of 46 m,

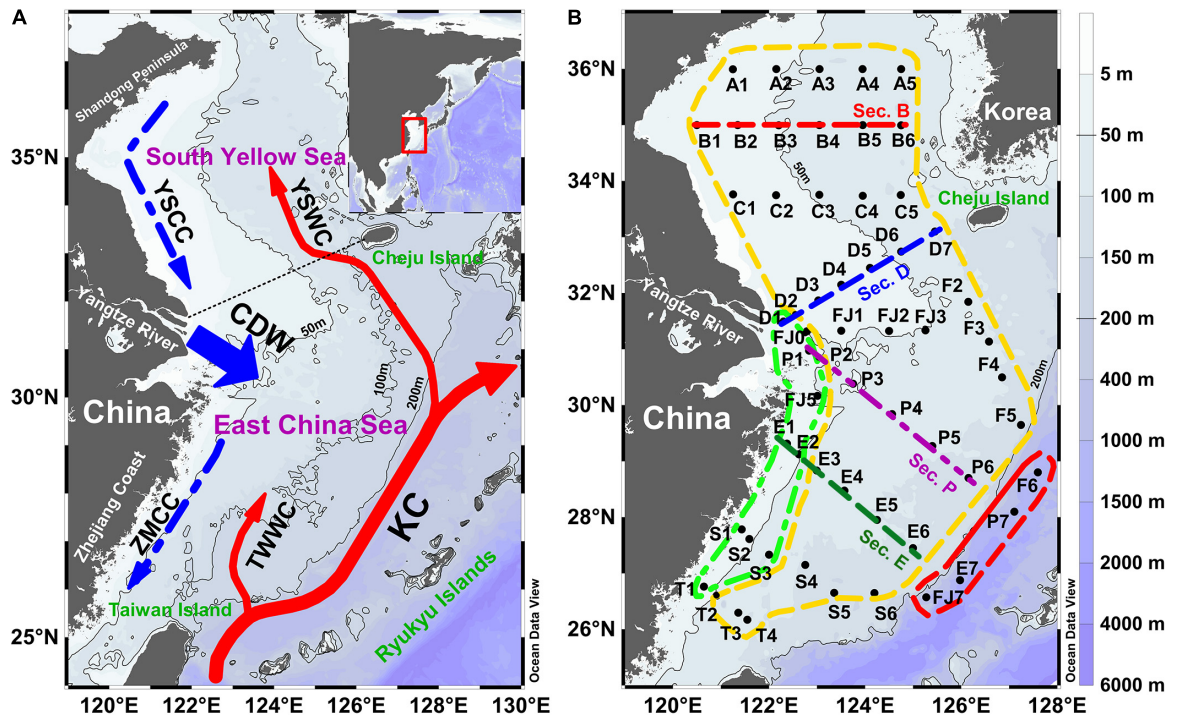

FIGURE 1 | The study area with **(A)** the regional hydrographic circulation and **(B)** sampling stations in the East China Sea (ECS) and the South Yellow Sea (SYS). The black dotted line represents the boundary between the ECS and the SYS. The major currents shown are KC (Kuroshio Current), TWWC (Taiwan Warm Current), YSWC (Yellow Sea Warm Current), YSCC (Yellow Sea Coastal Current), ZMCC (Zhe-Min Coastal Current), and CDW (Changjiang Diluted Water). The green, yellow, and red dashed polygonal boxes denote the nearshore region, the continental shelf region, and the slope region, respectively. The red, blue, purple, and green dashed lines denote sections B, D, P, and E, respectively.

characterized by a basin running from the north toward the southeast. The shallower and broader continental shelf, with an average depth of 66 m, is located in the west of the ECS, which occupies 66% of the whole ECS area (7.7×10^5 km^2). The deeper area (depth > 200 m) over the continental slope borders on the eastern edge of the shelf with a maximum depth of over 1,400 m. The water masses in the SYS and the ECS are characterized by coastal water, open ocean water, and mixed water between them (**Figure 1A**), with distinct seasonal characteristics (Quan et al., 2013; Lie and Cho, 2016). In early spring, driven by the East Asian Monsoon, the Yellow Sea coastal current (YSCC) flows southward along the western margin of the SYS, for which colder (<8°C) and lower salinity (<32.2 psu) water features prominently (Quan et al., 2013). With increasing runoff of the Yangtze River in spring, the less saline Changjiang Diluted Water (CDW) expands gradually and flows southeastward, driven by a northerly wind. As the largest terrestrial runoff for the ECS, the Yangtze River discharges over 9.04×10^{11} m^3 freshwater to the ECS every year (Chen et al., 2006), carrying massive loads of organic matter, nutrients, and sediment (Gao et al., 2015; Wang et al., 2015; Lin et al., 2017). A tongue with warm and saline water (T: 7–12°C, S: 32.5–34.3 psu) (Quan et al., 2013), carried by the Yellow Sea warm current (YSWC), penetrates northwestward from the Cheju Island to the SYS, which originates from the Tsushima warm current. Warmer and more saline tropical and subtropical water, characteristic of the Kuroshio current (KC), dominates the continental slope and flows northeast along the edge of the ECS. It plays an essential role in the ecological environment and circulation system with a high nutrient contribution to the marginal seas of China (Lie and Cho, 2016; Zhou et al., 2018). Moreover, the Taiwan warm current (TWWC) develops in the early spring and spreads to the middle of the ECS (Quan et al., 2013).

Field Sample and Chemical Analysis

Sampling took place onboard the R/V "Dong Fang Hong 2" in the SYS and the ECS during early spring (March 27–April 15, 2017). Hydrographic parameters of vertical profiles were obtained by sensors attached to a Seabird 911plus conductivity-temperature-depth (CTD) rosette system (Sea-Bird Electronics, Bellevue, WA, United States), and discrete water samples for chemical analysis were collected in 12-L Niskin bottles on the CTD rosette at 58 sampling stations (**Figure 1B**). Dissolved oxygen was measured onboard by the Winkler titration method (Hansen, 1999). Water samples for nutrient and chlorophyll-*a* (Chl-*a*) analysis were filtered using the 0.45 μm pore-size acetate cellulose filters and 0.7 μm pore-size Whatman GF/F filters, respectively, and stored under dark conditions at −20°C until analysis within 60 days. The Chl-*a* was determined according to Parsons et al. (1984) with a fluorescence spectrophotometer (Turner Designs, San Jose, CA, United States). The nutrients were determined, as described by Hansen and Koroleff (1999), with an auto-analyzer

(Seal Analytical, Norderstedt, Germany). The detection limit for ammonium, nitrite, and nitrate were 0.006, 0.005, and 0.02 μmol L^{-1}, respectively.

Subsamples for N_2O and NH_2OH were collected in duplicate from the Niskin bottles and put into 52.5 ml acid-washed glass serum bottles, and then 0.1–0.5 ml of the saturated mercuric chloride solution was added. These were immediately sealed using a butyl-rubber septum and aluminum cap without headspace. According to Kock and Bange (2013), the ferric ammonium sulfate (FAS) and sulfanilamide/acetic solution were injected into the NH_2OH subsamples after the addition of nitrogen headspace, and then the subsamples were stored in the dark for 24 h to ensure adequate oxidation of NH_2OH to N_2O before N_2O analysis. Subsequently, N_2O concentrations were quantified onboard using a gas chromatograph (HP6890, Agilent, United States) fitted with an electron capture detector (ECD) by the headspace equilibrium method (Zhang et al., 2010). Three-point calibration curves for ECD were constructed using three standard gas mixtures with an N_2O mixing ratio of 230, 610, and 3,040 ppb N_2O/N_2 (National Institute of Metrology, China), which had been calibrated against the primary gas standards prepared for the Working Group 143 of the Scientific Committee on Oceanic Research (SCOR) by John Bullister and David Wisegarver at the Pacific Marine and Environmental Laboratory (PMEL) of the National Oceanic and Atmospheric Administration (NOAA) (Wilson et al., 2018). The NH_2OH concentrations were computed according to the following equations:

$$[\boldsymbol{NH_2OH}] = ([\boldsymbol{N_2O}]_{\boldsymbol{FAS}} - [\boldsymbol{N_2O}]_{\boldsymbol{BG}})/\boldsymbol{RC} \quad (1)$$

$$\boldsymbol{RC} = \boldsymbol{m_{std}} \times 2 \quad (2)$$

where $[N_2O]_{FAS}$ and $[N_2O]_{BG}$ are the N_2O concentrations with and without the FAS conversion, respectively. The curve for determining NH_2OH recovery factor (RC) was generated from the NH_2OH standard additions of six different concentrations, which were made by the *in situ* seawater from the study area, and m_{std} stands for the regression slope of the standard curve. The NH_2OH RCs in the study area were relatively stable (63–69%) in the SYS and the ECS. The detection limit was 1.0 nmol L^{-1} for N_2O and 0.6 nmol L^{-1} for NH_2OH, respectively (Zhang et al., 2010; Kock and Bange, 2013; Ma et al., 2020).

Biogeochemical Calculations

The N_2O saturation (R, %) and flux (F, in μmol m^{-2} d^{-1}) across the air–sea interface were estimated with the following equations:

$$\boldsymbol{R} = \frac{[\boldsymbol{N_2O}]_{\boldsymbol{obs}}}{[\boldsymbol{N_2O}]_{\boldsymbol{eq}}} \times 100\% \quad (3)$$

$$\boldsymbol{F} = \boldsymbol{k} \times \left([\boldsymbol{N_2O}]_{\boldsymbol{obs}} - [\boldsymbol{N_2O}]_{\boldsymbol{eq}}\right) \quad (4)$$

where $[N_2O]_{obs}$ represents the observed concentration of N_2O, and $[N_2O]_{eq}$ is the estimated equilibrium concentration of N_2O in seawater with the *in situ* temperature, salinity, and the atmospheric N_2O concentration, according to the solubility parameterization derived from Weiss and Price (1980). However, the atmospheric N_2O concentrations were not measured in this study; instead, a monthly average atmospheric N_2O mixing ratio of 330.9 ppb in April 2017 was measured at two observation stations near the East China Sea (Lulin, Taiwan, 330.78 ppb; and Tae-ahn Peninsula, South Korea, 331.07 ppb) from the NOAA/ESRL Global Monitoring Division *in situ* program[1] was used for all calculations. The k (in length time^{-1}), gas transfer velocity, is a function of the Schmidt number (S_c) and the wind speed (in m s^{-1}). The wind speed was obtained on board and calibrated to 10 m above the surface according to Garratt (1977) (see **Supplementary Material** for details). The primary error in the flux estimation is derived from uncertainties in instantaneous gas transfer velocities. Due to a lack of direct data of gas transfer velocity in the SYS and the ECS, the parameterized relationship from Wanninkhof (2014) (referred to as W2014) and Nightingale et al. (2000) (referred to as N2000) were adopted to estimate k for comparison. Compared with the widely used formula of Wanninkhof (1992), the W2014 formula reflected the advances that have occurred over the past two decades. It can be applied to determine gas exchange at a broader range of temperatures (0–40°C) and intermediate winds (≈4–15 m s^{-1}). The N2000 formula is widely accepted and is used in estimating N_2O fluxes of the coastal ocean, including the ECS (Wang et al., 2016; Chen et al., 2021). Therefore, both N2000 and W2014 relationships were utilized to estimate the transfer velocity in this study.

Excess N_2O (ΔN_2O), a parameter to assess the apparent yield of N_2O in water, was calculated as the difference between the observed N_2O concentration and the atmospheric equilibrium concentration of N_2O in seawater. Apparent oxygen utilization (AOU) provides an indicator of the O_2 consumed by the organic matter remineralization and nitrification in water, and is calculated as the difference between the atmospheric equilibrium concentration of O_2 and its measured concentration (Nevison et al., 2003).

Based on Redfield stoichiometry (C: N: P = 106:16:1), N* reflects the nitrogen deficit or excess compared to phosphate in the ocean and was computed as the following equation according to Gruber and Sarmiento (1997):

$$\boldsymbol{N^*} = \left(\left[\boldsymbol{NH_4^+}\right] + \left[\boldsymbol{NO_2^-}\right] + \left[\boldsymbol{NO_3^-}\right] - 16\left[\boldsymbol{PO_4^{3-}}\right] + 2.9\right) \times 0.87 \quad (5)$$

where $[NH_4^+]$, $[NO_2^-]$, $[NO_3^-]$, and $[PO_4^{3-}]$ denote the concentrations (in μmol L^{-1}) of NH_4^+, NO_2^-, NO_3^-, and PO_4^{3-}.

Spearman correlation analysis and principal component analysis (PCA) were performed between the biogeochemical variables, using the SPSS 25.0 Statistics software (IBM Corp, United States). The significance level for all statistical analyses was $p < 0.05$.

RESULTS

To compare the hydrographic and biogeochemical variation, the study areas were divided into three subareas according to

[1] http://www.esrl.noaa.gov/gmd

the surface salinity distribution and bathymetric classification: the nearshore region (S < 31 psu), the continental shelf (S > 31 psu, depth < 200 m), and the slope (S > 34 psu, depth > 200 m) (**Figure 1B**).

Horizontal Distributions

Figure 2 shows the surface distributions of temperature, salinity, dissolved oxygen (DO), Chl-*a*, N_2O, NH_2OH, and N_2O saturations in the ECS and the SYS. Due to the spatial difference of solar radiation in early spring, there was a marked trend in the surface water temperature, characterized by a progressive north–south increasing gradient from ∼36 to ∼27°N (**Figure 2A**). The surface salinity in the ECS showed an offshore increasing trend with a minimum of 25.8 psu in the estuary of Yangtze River and a maximum of 34.9 psu in the continental slope (**Figure 2B**). The surface salinity had a relatively narrow range (31.1–33.4 psu) in the SYS, with a saline water tongue (S > 32.5 psu) of YSWC penetrating northward from the Cheju Island and reaching 35°N. This suggests that the Kuroshio current and the Taiwan warm current, carrying warmer and more saline waters, dominated the outer shelf and slope region. Low saline coastal water was prevalent over the nearshore region. Moreover, continental shelf-mixed water, which was formed by the mixing of the coastal current and open ocean water, covered the entire ECS continental shelf and extended northwestward to 32°N, to the Yangtze River estuary, with a remarkably warm water tongue (T > 12°C, S > 32.5 psu).

The DO showed a heterogeneous distribution in the study area, varying from 215 to 426 μmol L^{-1} (**Figure 2C**). Higher DO, up to over 320 μmol L^{-1}, was recorded along the Zhejiang coast and in the north of SYS, whereas lower values were observed on the continental slope. The extremums of Chl-*a*, which reached more than 4 μg L^{-1}, occurred in the same areas as high DO, but Chl-*a* appeared to be more horizontally uniform on the other areas with values lower than 1 μg L^{-1} (**Figure 2D**). The observed high Chl-*a* values, along with the cooccurrence of high DO, suggest the potential onset of phytoplankton blooms in early spring (Jin et al., 2013; Zhao et al., 2016).

The surface N_2O in the ECS ranged from 5.9 to 10.8 nmol L^{-1}, with a mean ± SD of 7.9 ± 1.1 nmol L^{-1} and characterized by an evident offshore decreasing trend, corresponding to 77–112% in saturation (**Figure 2E**). However, the surface N_2O in the SYS presented a relatively homogenous distribution with a narrow range of 8.4 to 11.3 nmol L^{-1} and a mean ± SD of 9.8 ± 0.8 nmol L^{-1}, which corresponds with a saturation of 75–97% (**Figure 2E**). As a whole, the surface N_2O concentrations decreased gradually with decreasing latitude in the study area. A wide range of NH_2OH was observed, from undetectable to 16.4 nmol L^{-1}, and had patchy characteristics in the SYS and the ECS. High NH_2OH levels over 5 nmol L^{-1} occurred along the coast of the Shandong peninsula and the Zhejiang coast (**Figure 2F**).

Vertical Profiles

To compare the biogeochemical diversity in different water layers, we measured depth profiles of hydrographic and biogeochemical parameters in typical transects.

The depth profiles of temperature, salinity, DO, Chl-*a*, N_2O, and NH_2OH of section B, a cross-shelf section in the middle of SYS, are shown in **Figure 3**. Owing to vertical mixing that continued from winter to early spring, the same trends were vertically uniform, which were apparent in both temperature and salinity in the SYS. The middle of transect B corresponded to the local maximum in both temperature and salinity, dominated by the YSWC; the colder and less saline waters, carried by the coastal current, occupied both sides of the cross transect. Both DO and Chl-*a* concentrations varied in a narrow range of 286–320 μmol L^{-1} and 0.07–1.98 μg L^{-1}, respectively, in transect B. Higher values were found in shallow water areas (Stations B1and B2) near the coast, which gradually decreased offshore. No straightforward pattern could be observed in the distribution of N_2O concentrations along transect B, with weak stratification in portions of transect B. The local N_2O extremum (∼10 nmol L^{-1}) occurred in the middle transect (Station B4), which was dominated by warm and saline water of YSWC; whereas the distribution of N_2O was not consistent with that of temperature and salinity, indicating that physical processes and water masses were not the only factors that influenced the N_2O distribution in the SYS. NH_2OH concentrations varied between undetectable and 5.2 nmol L^{-1} in the whole transect with no clear distribution pattern.

Transect D is located at the boundary between the SYS and the ECS. Temperature and salinity showed vertically uniform distributions in transect D, which featured the offshore increasing gradient (**Figure 4**). The effect of CDW was constrained only in a narrow area of the estuary (Station D1) in early spring, whereas the ECS continental shelf-mixed water penetrated the estuary with warm and saline water. The Chl-*a* profile at transect D showed vertical stratification, which decreased gradually from the surface maximum of 0.90 μg L^{-1} to below the detection limit at the bottom. The N_2O concentrations, varying from 7.0 to 10.8 nmol L^{-1}, appeared to be weakly stratified (**Figure 4**). The lower N_2O values were observed in the area where continental shelf-mixed water and open ocean water dominated, whereas the higher values occurred in the middle of transect D. The DO varied from 263 and 297 μmol L^{-1}, and followed a similar spatial distribution as described for N_2O (**Figure 4**).

Section P, extending southeastward from the Yangtze River estuary to the Kuroshio mainstream, is a representative coastal-oceanic section for biogeochemical research in the ECS. Wide ranges of temperature (from 13.0 to 21.9°C) and salinity (from 28.5 to 34.9 psu) were recorded along the cross-shelf section P (**Figure 5**). The Kuroshio current, carrying the warm (>15°C) and saline (>34.3 psu) water (Chen, 2009; Quan et al., 2013), dominated the offshore station and penetrated northwestward along the continental shelf, of which the impact reached to 50 m isobaths. Chl-*a* concentrations, coupled with DO, became stratified in transect P, decreasing steadily with depth, of which values ranged from 0.09 to 1.88 μg L^{-1} and 220 to 281 μmol L^{-1}, respectively (**Figure 5**). The concentrations of N_2O, varying from 6.2 to 9.4 nmol L^{-1}, showed a stratified pattern along transect P, and N_2O in the inshore water column was generally higher than that in the offshore stations (**Figure 5**). The local maximum N_2O in the upper layer of transect P, along with the concurrent greatest

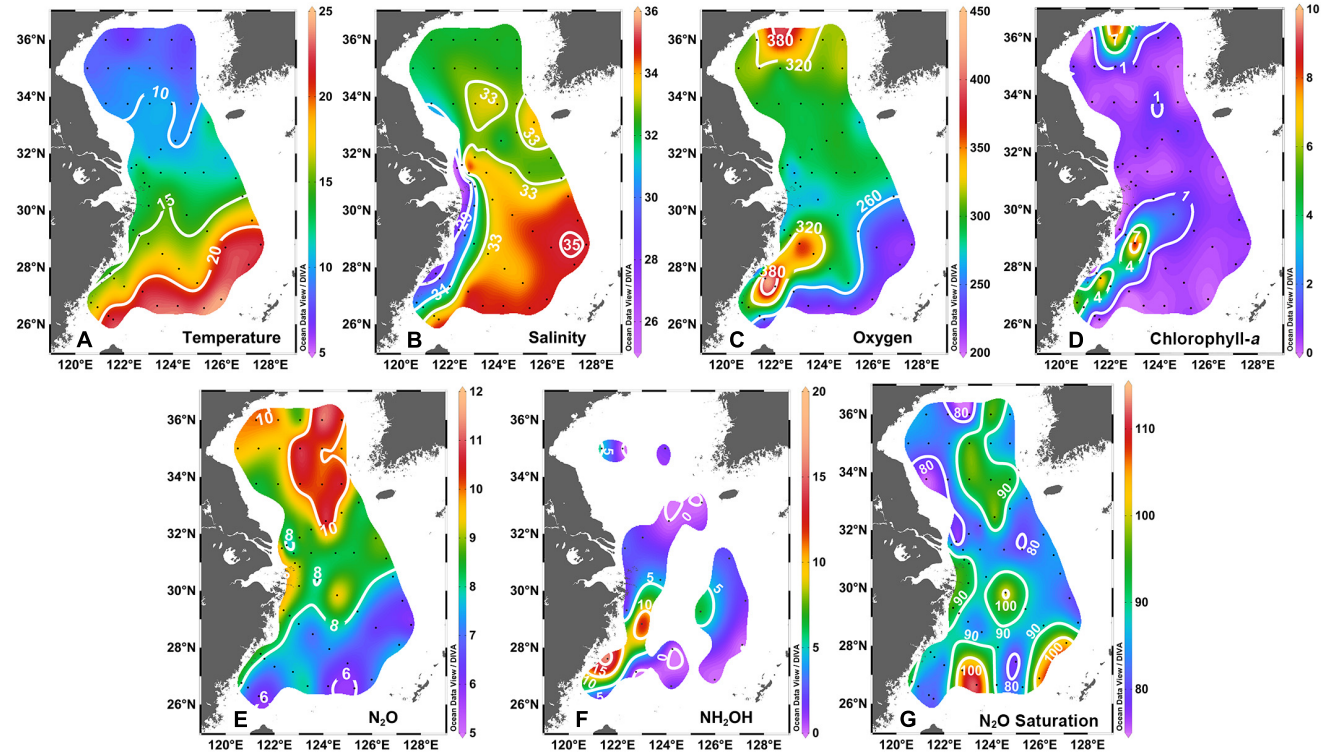

FIGURE 2 | The surface physical and biogeochemical distributions in the SYS and the ECS: **(A)** temperature (°C); **(B)** salinity (psu); **(C)** dissolved oxygen (μmol L^{-1}); **(D)** chlorophyll-*a* (μg L^{-1}); **(E)** N_2O (nmol L^{-1}); **(F)** NH_2OH (nmol L^{-1}); and **(G)** N_2O saturation (%).

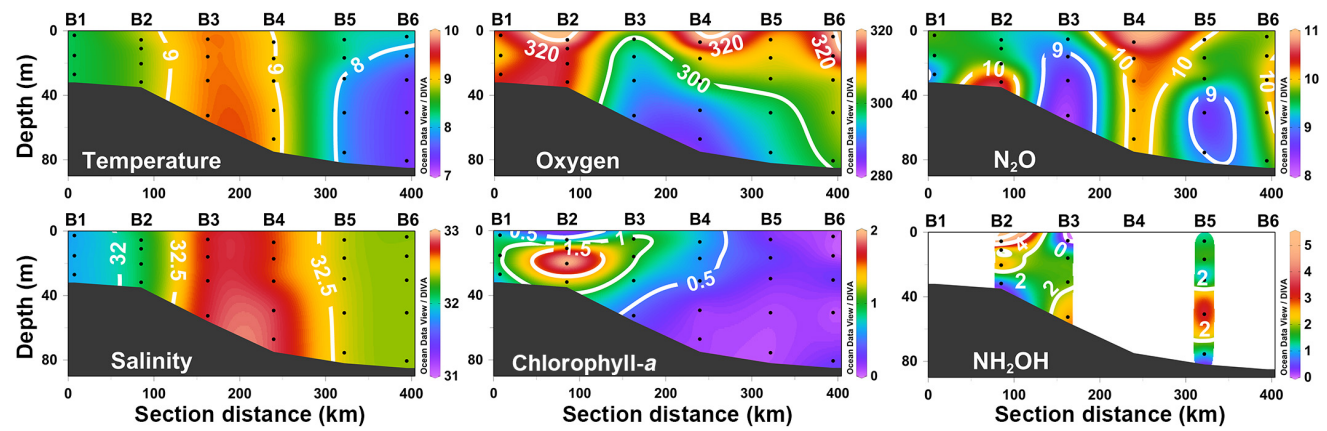

FIGURE 3 | The vertical distributions of temperature (°C), salinity (psu), dissolved oxygen (μmol L^{-1}), chlorophyll-*a* (μg L^{-1}), N_2O (nmol L^{-1}), and NH_2OH (nmol L^{-1}) along section B.

values of DO and Chl-*a* suggest the potential of aerobic microbial processes, associated with organic matter remineralization, for the N_2O production, such as nitrification. However, there was no apparent spatial pattern of the NH_2OH profile, and it was not consistent with the N_2O distribution in section P.

Section E spans the continental shelf of the ECS. The nearshore regions of section E (Stations E1 and E2) were dominated by colder and less saline waters of CDW, whereas the more saline water mass from the Kuroshio current penetrated the offshore regions of section E (**Figure 6**). The DO profile was stratified and decreased with increasing depth, where DO values varied from 186 to 360 μmol L^{-1}. A relatively narrow range of N_2O was recorded from 6.3 to 9.3 nmol L^{-1}, and regional maxima occurred in the coastal areas (Stations E1 and E2). The Chl-*a* concentrations were below the detection limit in most areas of section E, except the upper waters of stations E2, E3, and E4.

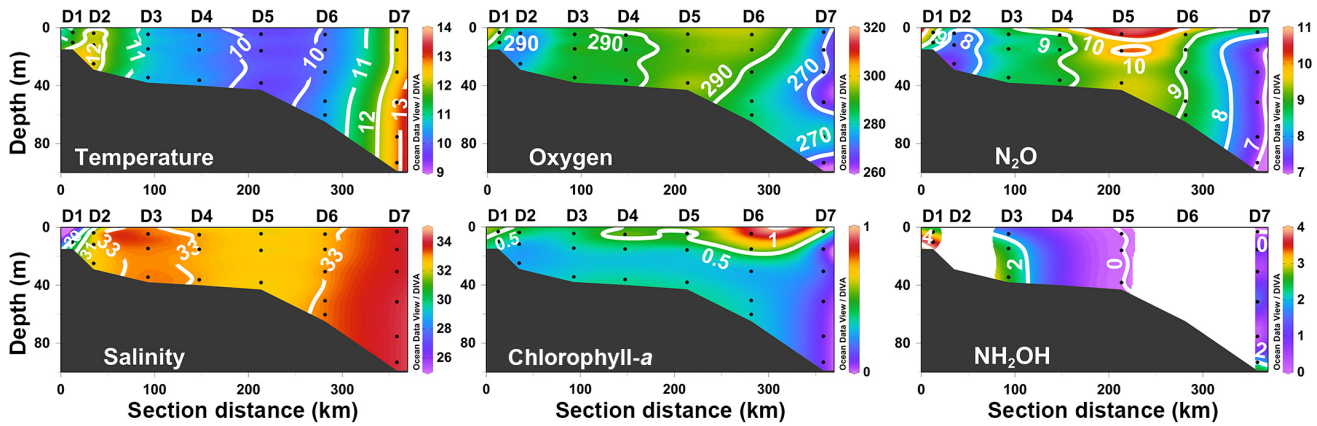

FIGURE 4 | The vertical distributions of temperature (°C), salinity (psu), dissolved oxygen (μmol L^{-1}), chlorophyll-*a* (μg L^{-1}), N_2O (nmol L^{-1}), and NH_2OH (nmol L^{-1}) along section D.

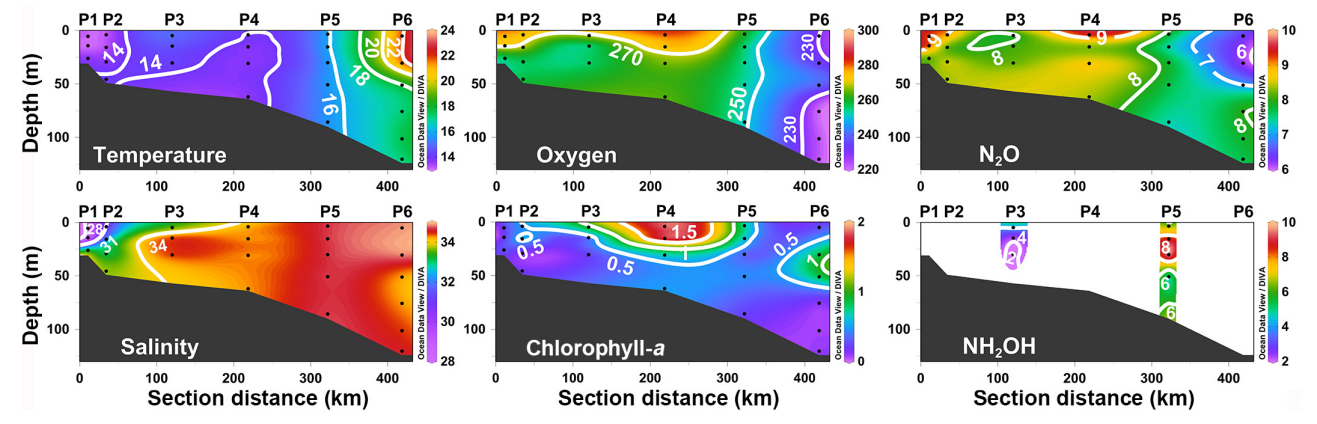

FIGURE 5 | The vertical distributions of temperature (°C), salinity (psu), dissolved oxygen (μmol L^{-1}), chlorophyll-*a* (μg L^{-1}), N_2O (nmol L^{-1}), and NH_2OH (nmol L^{-1}) along section P.

Similar to the Chl-*a* profile, the local maximum of NH_2OH values (>10 nmol L^{-1}) were observed in the surface water of station E3 (**Figure 6**).

Two profiles (Stations E7 and P7) of hydrographic properties, oxygen, Chl-*a*, N_2O, and NH_2OH, and also nitrogenous nutrients in the continental slope are shown in **Figure 7**. Similar patterns of the hydrographic and biogeochemical profiles at both stations revealed that the environmental perturbations were steady in the continental slope (**Supplementary Figure 1**). Temperature and salinity dropped from the mixed layer uniform values (~22°C and ~34.8 psu, respectively) to minima (~4°C and ~34.4 psu, respectively) in the deep waters. At both stations, the oxygen concentration was highest and homogenous (~220 μmol L^{-1}) in the mixed layer and decreased consistently throughout the water column to a minimum at the bottom (~90 μmol L^{-1}). The Chl-*a* peak was apparent in the upper waters, 0.09 μg L^{-1} at 75 m and 0.49 μg L^{-1} at 30 m, respectively, whereas it was low to undetectable below 800 m at either station. The shape of the N_2O profile was consistent with that of NO_3^-, and mirrored that of O_2 and N*, increasing gradually from the uniform values (~6 nmol L^{-1}) in the mixed layer water to the maxima (~30 nmol L^{-1}) below 800 m. Both NH_4^+ and NO_2^- were low and showed subsurface maxima at both stations. The NH_2OH concentrations fluctuated sharply with a wide range between undetectable and 4.8 nmol L^{-1}, showing a tripartite-peak structure at both stations.

DISCUSSION

To further examine the complex biogeochemical and physical processes of N_2O cycling, Spearman correlation analysis and PCA of N_2O, NH_2OH, and other environmental variables were performed on the whole water column samples in the SYS and the ECS. Different Spearman correlations among biogeochemical variables, including temperature, salinity, Chl-*a*, DO, NH_2OH, N_2O, and nitrogenous nutrients (i.e., NH_4^+, NO_2^-, and NO_3^-) are listed in **Table 1**. The distribution of N_2O in the study area was negatively correlated with temperature (**Table 1**, Rho = −0.794, $p < 0.05$, $n = 218$) and salinity (**Table 1**, Rho = −0.397, $p < 0.05$,

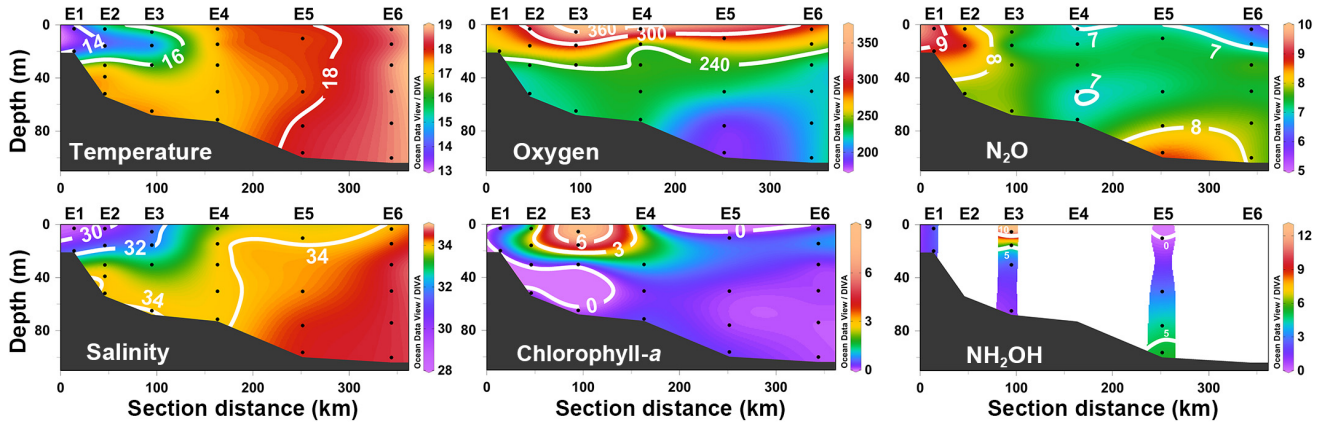

FIGURE 6 | The vertical distributions of temperature (°C), salinity (psu), dissolved oxygen (μmol L^{-1}), chlorophyll-*a* (μg L^{-1}), N_2O (nmol L^{-1}), and NH_2OH (nmol L^{-1}) along section E.

n = 218). Furthermore, as shown from the results of PCA (**Supplementary Tables 1, 2**), temperature and salinity, separated from N_2O, loaded highly on the same principal component (PC3) that only explained 17.8% of the variance, indicating that the controls of N_2O from physical factors were limited and not the primary factor in the study area. PC1 explained 31.5% of the variance (**Supplementary Table 1**) and had marked positive loadings for N_2O, AOU, and NO_3^- (**Supplementary Table 2**). Also, considering the correlations between N_2O concentrations and nitrogenous nutrients (**Table 1**), the nitrogen-related biochemical drivers regulating N_2O distribution cannot be ignored, particularly the aerobic microbial activities.

Regarding the NH_2OH distribution, however, no relationship with temperature and salinity could be established (**Table 1**), and we speculated that this could be due to the short residence time of NH_2OH (Butler et al., 1987, 1988) and rapid transformation via biochemical processes in seawaters. Moreover, a positive correlation between NH_2OH and Chl-*a* (**Table 1**, Rho = 0.329, $p < 0.05$, $n = 218$) was observed, implying that the production and accumulation of NH_2OH may be affected by phytoplankton activities directly or indirectly. It is noteworthy that there was no straightforward relationship neither between NH_2OH and N_2O concentrations nor between NH_2OH and the N_2O saturation (**Table 1**). The potential for NH_2OH production and accumulation will be discussed in detail below.

In order to distinguish the difference of physical and biochemical factors controlling N_2O and NH_2OH distributions in different biogeochemical environments, the data of the nearshore region, continental shelf, and the slope were analyzed, respectively.

Nearshore Region

The nearshore region covers the Yangtze River estuary and the Zhejiang coast, where it receives massive loading of organic material and nutrients from the Yangtze River and other terrigenous runoff (Cai et al., 2011). As shown in **Figure 2**, extreme Chl-*a* concentrations as high as over 4 μg L^{-1}, coinciding with high O_2 values (>320 μmol L^{-1}), occurred in the nearshore region, indicating the occurrence of a spring phytoplankton bloom. The considerable accumulation of NH_2OH in the nearshore area was coupled to the aerobic metabolic process associated with NH_4^+, i.e., ammonium oxidation, as indicated because the same principal component had high loadings from NH_2OH, Chl-*a*, AOU, and NH_4^+ (**Supplementary Table 3**). A previous study noted that the onset of the phytoplankton bloom in the ECS was usually in early spring (Shen et al., 2019). During the spring phytoplankton bloom, oxygenated conditions accompanying the enhanced Chl-*a* signaled the significance of primary productivity, leading to increased organic material and the subsequent remineralization, which was optimal for microorganism metabolism.

Ammonia-oxidizing archaea are ubiquitous in the shallow coastal water of the ECS and the Yangtze River estuary, and might play a vital role in ammonium oxidation (Zeng et al., 2007; Hu et al., 2013). Relative to AOB, AOA could maintain conspicuous tolerance to a low NH_4^+ environment (<1 μmol L^{-1}) and still sustain the high specific rate of ammonium oxidation (Martens-Habbena et al., 2009). AOA presents a strikingly higher affinity for reduced nitrogen than AOB and phytoplankton (Martens-Habbena et al., 2015). During the onset of the spring bloom, the dramatically increasing O_2 availability of up to over 250 μmol L^{-1} was optimal for NH_2OH production from ammonium oxidation driven by AOA (Martens-Habbena et al., 2009). There was a highly positive relationship between NH_2OH and NO_2^- (**Table 2**, Rho = 0.723, $p < 0.05$, $n = 21$), along with the negative relationship between NH_2OH and NO_3^- (**Table 2**, Rho = −0.709, $p < 0.05$, $n = 21$) observed in the nearshore area, and this can be interpreted as a sign that a "fresh" nitrifying system was established in the period of sharply increasing DO. It can be inferred that the first step of nitrification (ammonium oxidation) exceeded the second step rate (nitrite oxidation) and then favored the dynamic NH_2OH accumulation in a short time. These results are consistent with studies from the southwestern Baltic Sea, and Schweiger et al. (2007) also suggest that the rapidly increasing and accumulation of NH_2OH after reoxygenation of the water column can be interpreted as an indicator for the "fresh"

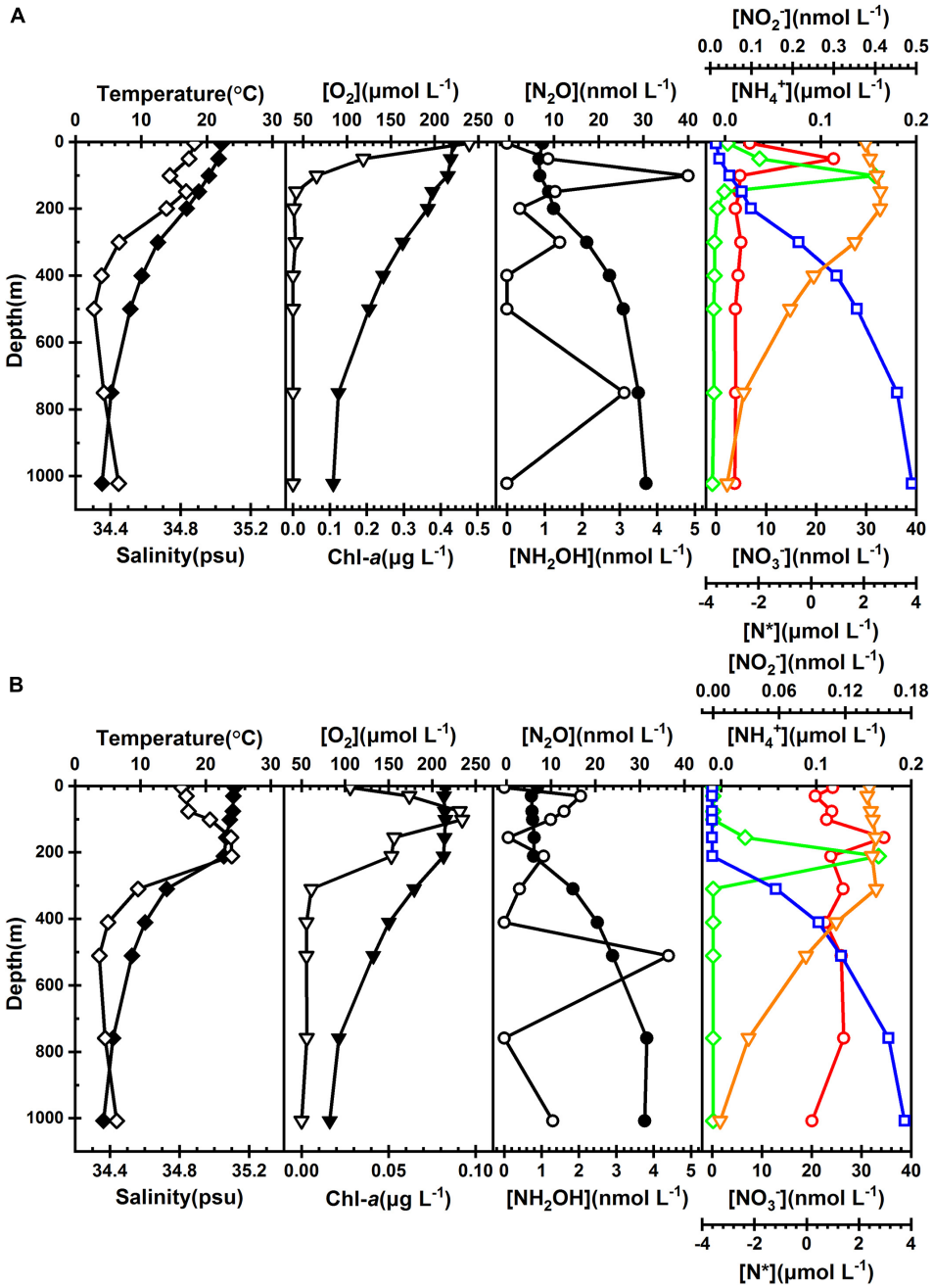

FIGURE 7 | The vertical profiles of temperature (°C, solid diamond), salinity (psu, open diamond), O_2 (μmol L^{-1}, solid triangle), chlorophyll-*a* (μg L^{-1}, open triangle), N_2O (nmol L^{-1}, solid cycle), NH_2OH (nmol L^{-1}, open cycle), NH_4^+ (μmol L^{-1}, red cycle), NO_2^- (μmol L^{-1}, green diamond), NO_3^- (μmol L^{-1}, blue square), and N^* (μmol L^{-1}, orange triangle) shown at two representative stations **(A)** P7 and **(B)** E7.

nitrifying system. Previous works in the coast and estuary have found that ammonium oxidation may be decoupled with nitrite oxidation due to the different oxygen sensitivity of ammonia-oxidizers and nitrite-oxidizers, leading to an imbalance of these rates (Laperriere et al., 2019).

It is worth noting, however, that N_2O did not show extremely high values similar to that of NH_2OH, and even a negative correlation (**Table 2**, Rho = −0.693, $p < 0.05$, $n = 21$) between N_2O and NH_2OH was found. Moreover, the correlation between N_2O saturation and NH_2OH also was not statistically significant in the nearshore region (**Table 2**). As no equivalent of AOB-like hydroxylamine oxidoreductase is identified in AOA, it might not produce N_2O through the NH_2OH pathway which is similar to AOB during ammonium oxidation (Walker et al., 2010; Vajrala et al., 2013; Stieglmeier et al., 2014), but instead through nitrifier denitrification or "hybrid formation" (that is, each N atom of

TABLE 1 | Spearman correlation coefficient matrix for biogeochemical parameters measured in the SYS and the ECS.

	N_2O	NH_2OH	T	S	DO	Chl-*a*	NH_4^+	NO_3^-	NO_2^-	N_2O saturation
N_2O	1.000									
NH_2OH	−0.219*	1.000								
T	−0.794*	0.105	1.000							
S	−0.397*	−0.127	0.649*	1.000						
DO	0.175*	0.154	−0.476*	−0.804*	1.000					
Chl-*a*	−0.167*	0.329*	0.000	−0.477*	0.634*	1.000				
NH_4^+	−0.372*	0.200*	0.334*	0.089	0.024	0.268*	1.000			
NO_3^-	0.652*	−0.034	−0.620*	−0.483*	0.018	−0.186*	−0.420*	1.000		
NO_2^-	−0.238*	0.533*	0.061	−0.283*	0.314*	0.406*	0.217*	0.036	1.000	
N_2O saturation	0.495*	−0.254	0.051	0.322*	−0.484*	−0.378*	−0.135*	0.236*	−0.364*	1.000

*The correlations were established based on the complete dataset (n = 218) obtained from all sampling stations. *Correlations are deemed significant at $p < 0.05$.*

TABLE 2 | Spearman correlation coefficient matrix for biogeochemical parameters measured in the nearshore, the continental shelf, and the slope regions.

		N_2O	NH_2OH	T	S	DO	Chl-*a*	NH_4^+	NO_3^-	NO_2^-	N_2O saturation
	N_2O	1.000									
	NH_2OH	−0.693*	1.000								
	T	−0.846*	0.588	1.000							
Nearshore	S	−0.580*	0.079	0.627*	1.000						
region[a]	DO	−0.059	0.359	0.037	−0.505*	1.000					
	Chl-*a*	−0.430	0.321	0.497*	0.033	0.702*	1.000				
	NH_4^+	−0.560*	0.480	0.601*	0.112	0.559*	0.890*	1.000			
	NO_3^-	0.835*	−0.709*	−0.882*	−0.724*	0.021	−0.471*	−0.569*	1.000		
	NO_2^-	−0.297	0.723*	0.245	−0.213	0.472	0.625*	0.627*	−0.181	1.000	
	N_2O saturation	0.505*	−0.498	−0.113	0.026	−0.282	−0.142	−0.215	0.106	−0.315	1.000
	N_2O	1.000									
	NH_2OH	−0.186	1.000								
	T	−0.793*	0.162	1.000							
Shelf	S	−0.568*	0.143	0.811*	1.000						
region[b]	DO	0.675*	−0.207	−0.866*	−0.851*	1.000					
	Chl-*a*	0.084	0.116	−0.148	−0.322*	0.363*	1.000				
	NH_4^+	−0.329*	0.301*	0.336*	0.173*	−0.176*	0.208*	1.000			
	NO_3^-	0.485*	−0.050	−0.535*	−0.491*	0.275*	−0.155	−0.454*	1.000		
	NO_2^-	−0.131	0.412*	0.054	0.024	−0.218*	0.044	0.158*	0.212*	1.000	
	N_2O saturation	0.351*	−0.067	0.228*	0.326*	−0.172*	−0.087	0.001	−0.069	−0.128	1.000
	N_2O	1.000									
	NH_2OH	−0.281	1.000								
	T	−0.975*	0.128	1.000							
Slope	S	−0.856*	0.109	0.838*	1.000						
region[c]	DO	−0.929*	0.101	0.925*	0.831*	1.000					
	Chl-*a*	−0.839*	0.227	0.830*	0.805*	0.874*	1.000				
	NH_4^+	−0.393*	0.011	0.433*	0.370*	0.355*	0.411*	1.000			
	NO_3^-	0.977*	−0.133	−0.980*	−0.866*	−0.951*	−0.848*	−0.414*	1.000		
	NO_2^-	−0.421*	0.018	0.370*	0.486*	0.518*	0.529*	0.036	−0.403*	1.000	
	N_2O saturation	0.992*	−0.299	−0.952*	−0.861*	−0.923*	−0.841*	−0.385*	0.964*	−0.466*	1.000

Correlations are deemed significant at $p < 0.05$. [a] n = 21. [b] n = 156. [c] n = 41.

N_2O comes, respectively, from NO_2^- and NH_4^+) under low oxygen conditions (Stieglmeier et al., 2014; Trimmer et al., 2016; Frame et al., 2017). However, the temporary increase of O_2 could mitigate N_2O production via nitrification and "hybrid formation" in the short term (Frame and Casciotti, 2010; Frame et al., 2017; Qin et al., 2017). Our results are comparable with those measured in the Bedford Basin, in which the N_2O production was mitigated or even suppressed by sharply increasing O_2 (Punshon and Moore, 2004).

Consequently, we speculated that a predominance of AOA among ammonia-oxidizing organisms occurred in the coastal zones during the onset of spring bloom and formed a "fresh"

nitrifying system to stimulate the temporary NH_2OH production and accumulation; the related N_2O production was mitigated by the dramatic increase of O_2. In addition, this inference is partly supported by the PCA results (**Supplementary Table 3**), which revealed that the N_2O production in the nearshore might be related to the biochemical processes associated with NO_2^- and NO_3^- instead of NH_4^+. However, we cannot exclude the possibility that the short-term production rate of NH_2OH may highly exceed that of its conversion to N_2O, and it subsequently led to the lack of accompanying N_2O increase. Another possible reason was that the signal of the *in situ* N_2O production, which was not strong enough because of the high DO levels, may be masked by other biogeochemical processes, such as terrestrial runoff and anthropogenic inputs, that could arise due to the change of N_2O concentrations.

Unlike the open ocean, the biochemical processes and controls of nitrogen cycling in coastal areas are more complex; the relationship between N_2O and NH_2OH is not straightforward. Previous studies found that dissolved N_2O concentrations did not show any significant relationship with NH_2OH in the Baltic Sea (Schweiger et al., 2007), Indian Ocean (Ma et al., 2020), and the coastal region of the eastern tropical South Pacific Ocean (Korth et al., 2019). Butler et al. (1987) observed the apparent correlation between N_2O and NH_2OH in a coastal basin while stating that their correlation does not necessarily indicate the direct relationship between their production levels.

Continental Shelf

The continental shelf region extends southward from the coast of the Shandong Peninsula of China (36°N) to the Taiwan Strait (26°N), covering most of the ECS and the SYS (**Figure 1B**). Water temperature and N_2O loaded highly to the same principal component (**Supplementary Table 4**), with a highly negative relationship between them (**Table 2**, Rho = −0.793, $p < 0.05$, $n = 156$), suggesting that temperature was the important physical factor controlling the distribution of N_2O in the continental shelf. Such mirrored covariation between temperature and N_2O was especially evident in the surface distribution (**Figure 2**). In early spring, the surface temperature in the continental shelf exhibited a robust latitudinal gradient, increasing southward with a maximum temperature difference of 16.3°C. As previously mentioned (Weiss and Price, 1980), the solubility of N_2O in seawaters gradually decreases, in conjunction with increasing water temperatures. Therefore, the N_2O distribution in the continental shelf mirrored that of temperature, both in surface waters and depth profiles. Besides, a previous study reported that temperature appeared to be the primary control responsible for the N_2O production under nitrifying conditions (Humbert et al., 2020).

Hydroxylamine in the shelf waters was produced by ammonium oxidation, as indicated by the positive correlations of NH_2OH vs. NH_4^+ and NH_2OH vs. NO_2^- (**Table 2**, Rho = 0.301, $p < 0.05$, $n = 70$ and Rho = 0.412, $p < 0.05$, $n = 70$, respectively). Besides temperature, both NH_4^+ and NO_3^- loaded highly to the same principal component as N_2O (**Supplementary Table 4**), supporting N_2O production via nitrification. Dissolved NH_2OH presented low values (or even below the detection limit) at most continental shelf stations, and there was no correlation between N_2O and NH_2OH, indicating that the NH_2OH pathway, i.e., ammonium oxidation, was not the only main microbial process for the N_2O production in continental shelf waters. Considering the oxygen level in shelf waters, the contribution of denitrification to N_2O production can be excluded here. Hence, we speculated that the reduction of NO_2^-, i.e., nitrifier denitrification, might play an important role in the N_2O production besides ammonium oxidation.

Continental Slope

The Kuroshio current, which originates from the northward bifurcation of the North Equatorial Current, dominates the water masses in the continental slope areas. Contrasting sharply with those in the shelf regions, the hydrologic and biogeochemical characteristics in the continental slope are relatively stable and like those in open seas.

Although the evident triple-peak structures were recorded at both continental slope stations (**Figure 7**), dissolved NH_2OH concentrations did not show any significant relationships with N_2O or other variables (**Table 2**), comparable with the finding of Ma et al. (2020) in the Southwest Indian Ocean.

As observed in this study and others (Grundle et al., 2012), the significant relationships of ΔN_2O vs. AOU and ΔN_2O vs. NO_3^- (**Figures 8A,B**) in the whole water column have been interpreted as signs that the aerobic processes associated with NO_3^- were coupled to the N_2O production processes, that is, the N_2O production via nitrification. As the oxygen level in the continental slope highly exceeded the threshold for denitrification – reported as 2–10 μmol L^{-1} by Bange et al. (2010) – the potential of *in situ* incomplete denitrification for N_2O production can be ruled out. Therefore, we concluded that nitrification played a vital role in the N_2O production in the water mass over the continental slope.

According to the significant stratified structure of environmental variables in the continental slope, we investigated the distinction of the potential N_2O production pathways in different layers by analyzing the correlations between ΔN_2O and four of its related factors: AOU, NO_2^-, NO_3^-, and N* (**Figure 8**). AOU and NO_3^- in the upper waters (depth < 200 m) showed relatively weak and positive correlations with ΔN_2O, with coefficients 0.0345 (**Figure 8A**, $R^2 = 0.38$, $p < 0.05$, $n = 17$) and 0.2674 (**Figure 8B**, $R^2 = 0.43$, $p < 0.05$, $n = 17$), respectively. Thus, the slope of the ΔN_2O vs. AOU relationship can be interpreted as that 29,000 moles of O_2 are consumed per mole of N_2O produced, whereas that of the ΔN_2O vs. NO_3^- indicates that per mole of N_2O produced is linked to 3,740 moles NO_3^- produced. The N_2O yields from nitrification (0.020%), namely the molar ratio of N_2O production to NH_4^+ consumption, based on the correlation between ΔN_2O and AOU was below that (0.027%) based on the slope of ΔN_2O vs. NO_3^-. Along with the relatively weak correlation between them, it can be inferred that nitrification was not the only source and played a limited role in the N_2O production in upper waters. The absence of relationships between ΔN_2O and either NO_2^- or N* (**Figures 8C,D**), and the positive values of N* (>2.1 μmol L^{-1}) suggest the lack of a denitrification signal. The upper mixed layer in the continental slope corresponded to the shallow local

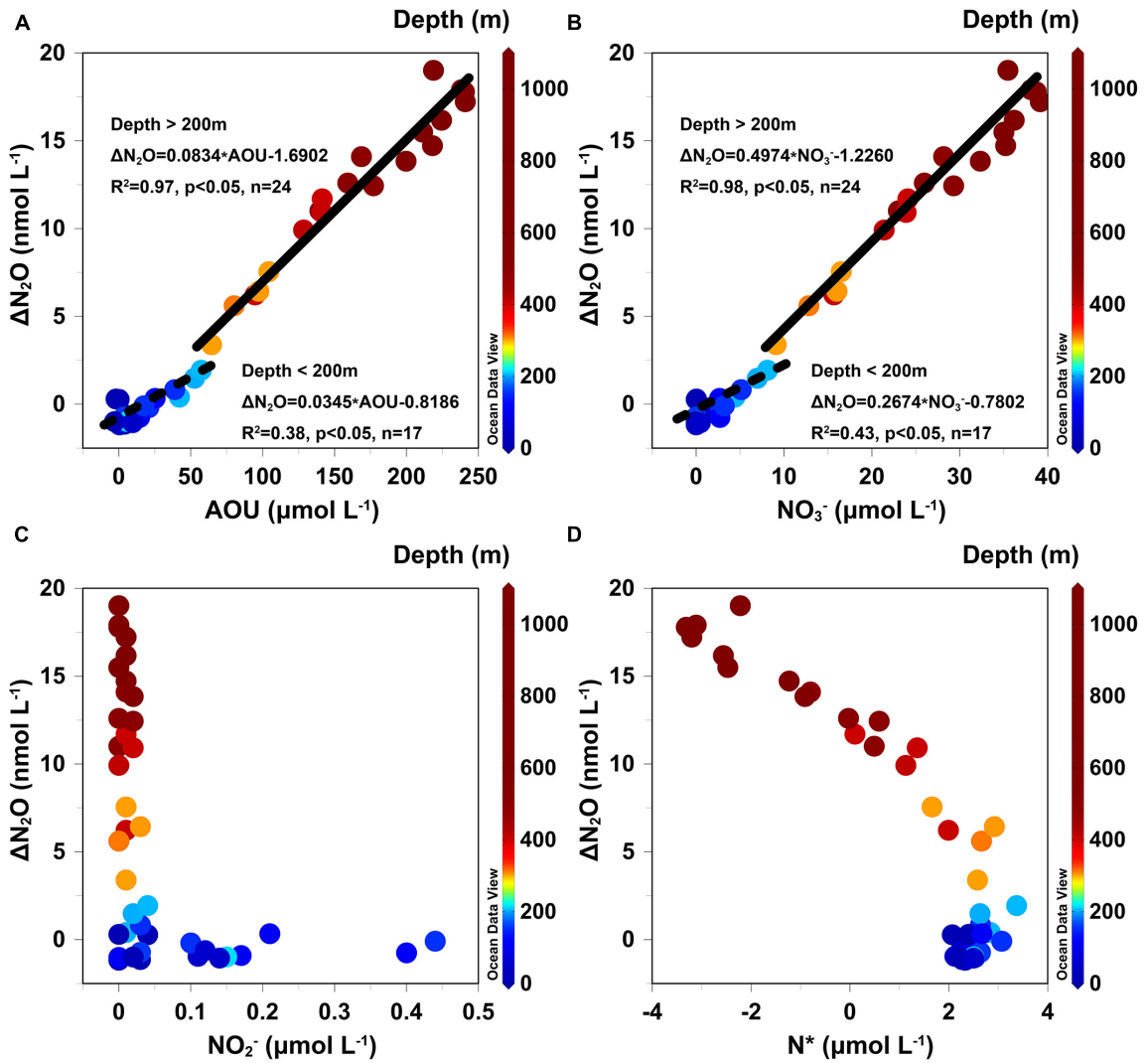

FIGURE 8 | The relationships **(A)** ΔN_2O vs. AOU; **(B)** ΔN_2O vs. NO_3^-; **(C)** ΔN_2O vs. NO_2^-; and **(D)** ΔN_2O vs. N* in the continental slope water columns. The dashed line and the solid line indicate the linear regression curve for datasets from the upper waters (<200 m) and the intermediate and deeper waters (>200 m). The color bar shows the water depth (m).

maxima in both NO_2^- ($\sim 0.4\ \mu mol\ L^{-1}$) and NH_4^+ ($\sim 0.2\ \mu mol\ L^{-1}$), along with gradual increases of N_2O levels (**Figure 7**). This suggests that nitrifier denitrification may contribute to the N_2O production in addition to nitrification in upper waters. This is consistent with previous studies of the North Pacific Ocean (Wilson et al., 2014) and the South China Sea (Zhang et al., 2019), where the contribution of nitrifier denitrification was also noted and even was purported as the main source for the N_2O production at the euphotic zone.

Regarding the intermediate and deep waters (depth > 200 m), highly positive correlations of ΔN_2O vs. AOU (**Figure 8A**, $R^2 = 0.97$, $p < 0.05$, $n = 24$) and ΔN_2O vs. NO_3^- (**Figure 8B**, $R^2 = 0.98$, $p < 0.05$, $n = 24$) were found, and the N_2O yields of nitrification calculated from slopes of these two relationships were similar (~0.049%), revealing that nitrification dominated the N_2O production in the intermediate and deep waters. Furthermore, the deficient level of NO_2^- does not support the potential of nitrite reduction, namely nitrifier denitrification, for the N_2O production in the intermediate and deep waters. These results are consistent with studies from the South China Sea (Zhang et al., 2019) and the western North Pacific (Breider et al., 2015).

Below 200 m, N* dropped steadily from its surface values of ~2.2 $\mu mol\ L^{-1}$ to a minimum of $-3.2\ \mu mol\ L^{-1}$ at 1,000 m. The negative N* values observed in deep waters are likely not the *in situ* denitrification signals because of the high level of O_2. Studies of the Northwest Pacific Ocean (Breider et al., 2015) and the West Philippines Sea (Tseng et al., 2016), both of which are located on the mainstream of Kuroshio, showed similar measured N* ($<-2.0\ \mu mol\ L^{-1}$) and N_2O values (20–30 $nmol\ L^{-1}$) at 800–1,000 m. In the eastern subtropical North Pacific, similar values to our work, ranging from 17.1

TABLE 3 | Overview of surface N_2O saturation (R), wind speed (U_{10}), and N_2O sea-to-air flux (F) in the SYS, and the nearshore, shelf, and slope area of the ECS.

	n	R (%)	U_{10} (m s^{-1})	F_{N2000} (μmol m^{-2} d^{-1})	F_{W2014} (μmol m^{-2} d^{-1})
SYS	16	86 ± 7	5.8 ± 3.1	−2.6 ± 2.9	−2.5 ± 3.1
Nearshore area of ECS	9	90 ± 4	9.7 ± 2.9	−4.8 ± 3.5	−5.0 ± 3.8
Shelf area of ECS	29	87 ± 8	8.4 ± 2.8	−4.4 ± 4.0	−4.5 ± 4.2
Slope area of ECS	4	95 ± 11	8.0 ± 3.2	−2.6 ± 4.8	−2.7 ± 5.0

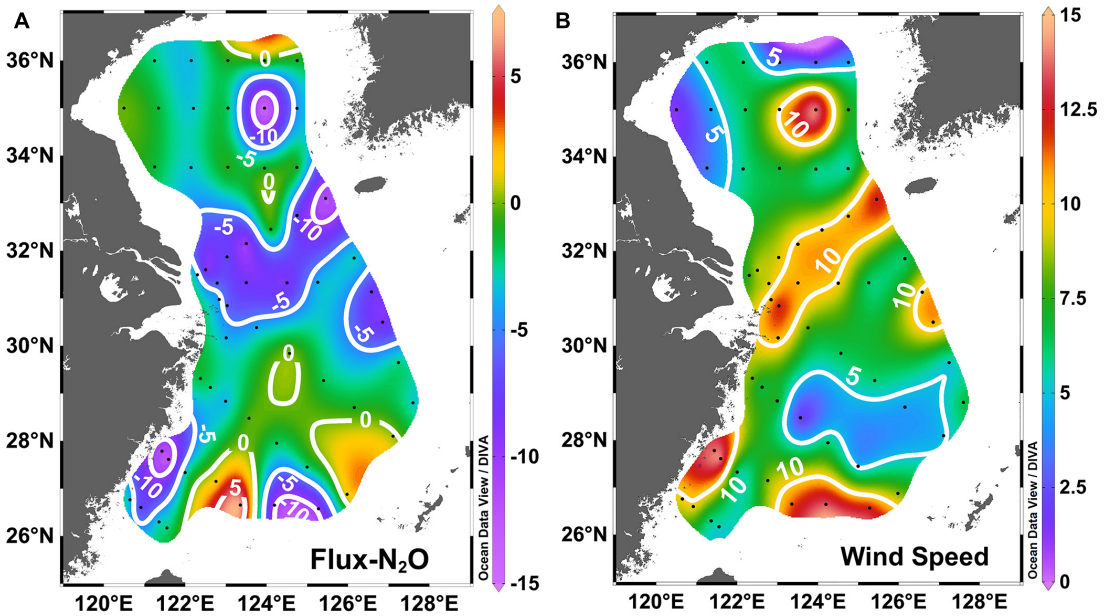

FIGURE 9 | (A) The sea-to-air flux of N_2O (μmol m^{-2} d^{-1}) and **(B)** wind speed (m s^{-1}) in the SYS and the ECS during early spring.

to 22.4 nmol L^{-1} of N_2O and −1.6 to −1.8 μmol L^{-1} of N^* were recorded (Fujii et al., 2013). Taking these into account, another potential interpretation is the far-field lateral advective transport of denitrification signals, carried by the Kuroshio current, from the western Pacific Ocean or even the remote eastern subtropical North Pacific Ocean. Fenwick and Tortell (2018) and Zhang et al. (2019) also proposed this potential source of lateral transport supply for deep N_2O in the South China Sea and the Northeast Subarctic Pacific, respectively. Consequently, we concluded that the primary sources of N_2O in deep water are nitrification and the advective transport from other areas.

The relationships between ΔN_2O and environmental variables, along with the distributions of dissolved N_2O and NH_2OH, provide some insights into the associated environmental controlling factors of the N_2O production and emission. However, because of the inherent limitations of analytical methods, the relevant microorganisms or inner mechanisms of the N_2O biogeochemical cycling were poorly defined. To explore and quantify the microbial processes for the N_2O production in various coastal areas, it is necessary to adopt multiple methodological approaches in the future, including isotopic and microbial analysis.

Sea to Air Flux of N_2O

During the early spring of 2017, surface N_2O saturations in the SYS and the ECS varied between 75 and 112% with a mean value of 88 ± 8%, suggesting the ECS and the SYS behaved overall as a sink of N_2O to the atmosphere (**Figure 2G**). The surface saturations of N_2O in marginal seas of China fluctuated from undersaturated to supersaturated levels throughout the whole year as previously reported (Yang et al., 2009; Chen et al., 2021). Prior studies showed that the surface N_2O saturations were slightly supersaturated in the SYS (122%) and the ECS (114–122%), acting as net sources of atmospheric N_2O in May 2011 (Chen et al., 2021). During our investigation, the N_2O appeared to be near equilibrium with the atmosphere, or even supersaturated, in individual stations of the central and southern ECS (**Figure 2G**). This shows that the strength of the N_2O sink was weakening. Therefore, we suggest that the SYS and the ECS in the early spring of 2017 acted overall as a sink of the atmospheric N_2O, whereas the strength was weakening.

Although presenting similar surface N_2O saturations, the subregions of the study area exhibited spatial variability in their sea-to-air fluxes of N_2O (**Table 3** and **Figure 9A**). This spatial variability was linked to the difference in the wind speed, one of the critical factors of sea-to-air flux. In early spring, the wind speed in the ECS and the SYS showed high spatial variability

(**Figure 9B**). Besides the wind speed, the surface N_2O saturation is another key factor. While high wind speed occurred in the continental slope area, the sea-to-air flux of N_2O was lower than that in other subregions due to near equilibrium with the atmosphere in surface water.

However, air–sea fluxes of N_2O in the subregions of the ECS and the SYS reported here were different from those observed by Chen et al. (2021) for March (4.5 ± 6.5 μmol m^{-2} d^{-1} in the SYS and 6.6 ± 9.5 μmol m^{-2} d^{-1} in the shelf of ECS, using the W2014 formula) and May (7.7 ± 4.6 μmol m^{-2} d^{-1} in SYS, 6.7 ± 8.0 μmol m^{-2} d^{-1} in the shelf of ECS and 5.6 ± 3.4 μmol m^{-2} d^{-1} in the slope of ECS, using the W2014 formula) in 2011. Biogeochemical cycling in the coastal system is highly variable and more susceptible to human-driven perturbations; yet, the results might be double-edged, either enhanced or inhibited. This change may only become apparent over the years, or even decades, of continuous observation. For example, Farías et al. (2015) found that the N_2O concentrations and fluxes showed apparent interannual variation in the coastal area off central Chile during 10 years of observation. In addition, with the continuous implementation of environmental protection measures, anthropogenic organic pollutants, nutrient inputs, and other negative anthropogenic impacts to coastal ecosystems may be reduced in the future. Prior long-term observations of the Baltic Sea (Ma et al., 2019) noted that low-N_2O-concentration events have become more frequent and suggest a potential decline of air–sea N_2O fluxes, which may be because of the gradual reduction of nutrient loading and eutrophication. In addition to the sea-to-air flux, the surface N_2O concentrations from our results were lower compared to those observed in the corresponding period in 2011 [13.1 and 11.7 nmol L^{-1} in the SYS and the ECS, respectively, see Chen et al. (2021)]. During the past decade, there were various possible reasons for the shifting N_2O levels, including the variability of climatological and environmental factors and human-driven perturbations, among many other factors.

Compared to the open ocean, hydrologic and biochemical variabilities in coastal areas are more complex, and it is difficult to assess the seasonal variation of sea-to-air fluxes more precisely. Given the short time of observation at each station during our cruise, the data collection could have been influenced by sudden meteorological and hydrologic events, such as variable winds and tidal current speeds, leading to uncertainty in the assessment of the seasonal N_2O emission to some extent. Even so, the spatial patterns and direction of air–sea N_2O fluxes are reasonable, yet it is critical to supplement the seasonal and interannual data sets of N_2O emissions in the coastal areas. To characterize the spatial and temporal patterns of N_2O in coastal areas and minimize uncertainty, it is necessary to build a long-term and continuous observation network in the future.

CONCLUSION

Our early spring observations of the N_2O and NH_2OH provide important insights into the underlying patterns, mechanisms, and controlling factors in the SYS and the ECS. During the spring phytoplankton bloom in the nearshore region, stimulated by the remineralization of organic matter and the increased oxygen level, a "fresh" nitrifying system was established, favoring the temporal production and accumulation of NH_2OH by the ammonia-oxidizing microorganisms. There was no straightforward relationship between N_2O and NH_2OH in this region. Dissolved N_2O in the SYS and the ECS can be potentially produced via nitrification and nitrifier denitrification. Besides, the lateral advective transport through the Kuroshio current provided the other source to N_2O in the intermediate and deep waters in the continental slope. Isotopic and microbiological studies are needed to provide more evidence for definitively identifying the biogeochemical processes of N_2O in this area.

Compared with previous N_2O observations, the SYS and the ECS in the early spring of 2017 acted overall as a sink of the atmospheric N_2O, whereas the strength was weakening. This was potentially related to biogeochemical diversity of coastal areas and supports, in part, a view that global oceanic N_2O emissions will probably have a declining trend into the future. However, owing to the lack of continuous observations, some key processes and variabilities of environmental characteristics might have been missed, masking key biogeochemical controls of coastal N_2O cycling. Long-term continuous observation would provide insight into the interannual trends of N_2O emissions in the marginal seas of China, which are affected by extensive anthropogenic perturbations and complex natural phenomena.

DATA AVAILABILITY STATEMENT

The datasets presented in this study can be found in online repositories. The names of the repository/repositories and accession number(s) can be found below: http://mds.nmdis.org.cn.

AUTHOR CONTRIBUTIONS

XG and GZ conceived and designed the research. XG, FC, and GD performed the fieldwork and measurements onboard. XG conducted the data analysis and wrote the original draft. XG, XC, and GZ participated in the revision of the manuscript. GZ provided the funding for the work. All authors read and approved the submitted version.

FUNDING

This work was supported by grants from the Ministry of Science and Technology of China (Grant Number: 2016YFA0601302) and the National Natural Science Foundation of China (Grant Numbers: U1806211 and 41776122).

ACKNOWLEDGMENTS

The authors sincerely appreciate the R/V "Dong Fang Hong 2" crew for their cooperation onboard. Special thanks to Liang Zhao

(Tianjin University of Science and Technology), Guipeng Yang (Ocean University of China), Yahui Gao (Xiamen University), and Yu Xin and Xiaosong Zhong (Ocean University of China) for providing hydrographic, dissolved oxygen, chlorophyll-*a*, and nutrient datasets.

SUPPLEMENTARY MATERIAL

The Supplementary Material for this article can be found online at: https://www.frontiersin.org/articles/10.3389/fmars.2021.725713/full#supplementary-material

REFERENCES

Bange, H. W., Arevalo-Martinez, D. L., DelaPaz, M., Farias, L., Kaiser, J., Kock, A., et al. (2019). A harmonized nitrous oxide (N_2O) ocean observation network for the 21st Century. *Front. Marine Sci.* 6:157. doi: 10.3389/fmars.2019.00157

Bange, H. W., Freing, A., Kock, A., and Löscher, C. R. (2010). "Marine pathways to nitrous oxide," in *Nitrous Oxide and Climate Change*, ed. K. Smith (Milton Park: Routledge), 36–62.

Battaglia, G., and Joos, F. (2018). Marine N_2O emissions from nitrification and denitrification constrained by modern observations and projected in multimillennial global warming simulations. *Glob. Biogeochem. Cycles* 32, 92–121. doi: 10.1002/2017gb005671

Breider, F., Yoshikawa, C., Abe, H., Toyoda, S., and Yoshida, N. (2015). Origin and fluxes of nitrous oxide along a latitudinal transect in western North Pacific: controls and regional significance. *Glob. Biogeochem. Cycles* 29, 1014–1027. doi: 10.1002/2014GB004977

Buitenhuis, E. T., Suntharalingam, P., and Le Quere, C. (2018). Constraints on global oceanic emissions of N_2O from observations and models. *Biogeosciences* 15, 2161–2175. doi: 10.5194/bg-15-2161-2018

Butler, J. H., Jones, R. D., Garber, J. H., and Gordon, L. I. (1987). Seasonal distributions and turnover of reduced trace gases and hydroxylamine in Yaquina Bay. *Oregon. Geochimica et Cosmochimica Acta* 51, 697–706. doi: 10.1016/0016-7037(87)90080-9

Butler, J. H., Pequegnat, J. E., Gordon, L. I., and Jones, R. D. (1988). Cycling of methane, carbon monoxide, nitrous oxide, and hydroxylamine in a meromictic, coastal lagoon. *Estuar. Coast. Shelf Sci.* 27, 181–203. doi: 10.1016/0272-7714(88)90089-3

Cai, W.-J., Hu, X., Huang, W.-J., Murrell, M. C., Lehrter, J. C., Lohrenz, S. E., et al. (2011). Acidification of subsurface coastal waters enhanced by eutrophication. *Nature Geosci.* 4, 766–770. doi: 10.1038/ngeo1297

Chen, C. T. A. (2009). Chemical and physical fronts in the Bohai. Yellow and East China seas. *J. Marine Syst.* 78, 394–410. doi: 10.1016/j.jmarsys.2008.11.016

Chen, S.-L., Zhang, G.-A., Yang, S.-L., and Shi, J. Z. (2006). Temporal variations of fine suspended sediment concentration in the Changjiang River estuary and adjacent coastal waters, China. *J. Hydrol.* 331, 137–145. doi: 10.1016/j.jhydrol.2006.05.013

Chen, X., Ma, X., Gu, X., Liu, S., Song, G., Jin, H., et al. (2021). Seasonal and spatial variations of N_2O distribution and emission in the East China Sea and South Yellow Sea. *Sci. Total Environ.* 775:145715. doi: 10.1016/j.scitotenv.2021.145715

Doney, S. C. (2010). The growing human footprint on coastal and open-ocean biogeochemistry. *Science* 328, 1512–1516. doi: 10.1126/science.1185198

Farías, L., Besoain, V., and García-Loyola, S. (2015). Presence of nitrous oxide hotspots in the coastal upwelling area off central Chile: an analysis of temporal variability based on ten years of a biogeochemical time series. *Environ. Res. Lett.* 10:44017. doi: 10.1088/1748-9326/10/4/044017

Fenwick, L., and Tortell, P. D. (2018). Methane and nitrous oxide distributions in coastal and open ocean waters of the Northeast Subarctic Pacific during 2015–2016. *Marine Chem.* 200, 45–56. doi: 10.1016/j.marchem.2018.01.008

Frame, C. H., and Casciotti, K. L. (2010). Biogeochemical controls and isotopic signatures of nitrous oxide production by a marine ammonia-oxidizing bacterium. *Biogeosciences* 7, 2695–2709. doi: 10.5194/bg-7-2695-2010

Frame, C. H., Deal, E., Nevison, C. D., and Casciotti, K. L. (2014). N_2O production in the eastern South Atlantic: Analysis of N_2O stable isotopic and concentration data. *Glob. Biogeochem. Cycles* 28, 1262–1278. doi: 10.1002/2013gb004790

Frame, C. H., Lau, E., Nolan, E. J. T., Goepfert, T. J., and Lehmann, M. F. (2017). Acidification enhances hybrid N_2O production associated with aquatic ammonia-oxidizing microorganisms. *Front. Microbiol.* 7:2104. doi: 10.3389/fmicb.2016.02104

Fujii, A., Toyoda, S., Yoshida, O., Watanabe, S., Sasaki, K. I, and Yoshida, N. (2013). Distribution of nitrous oxide dissolved in water masses in the eastern subtropical North Pacific and its origin inferred from isotopomer analysis. *J. Oceanograp.* 69, 147–157. doi: 10.1007/s10872-012-0162-4

Ganesan, A. L., Manizza, M., Morgan, E. J., Harth, C. M., Kozlova, E., Lueker, T., et al. (2020). Marine nitrous oxide emissions from three eastern boundary upwelling systems inferred from atmospheric observations. *Geophys. Res. Lett.* 47:87822. doi: 10.1029/2020gl087822

Gao, L., Li, D., Ishizaka, J., Zhang, Y., Zong, H., and Guo, L. (2015). Nutrient dynamics across the river-sea interface in the Changjiang (Yangtze River) estuary-East China Sea region. *Limnol. Oceanograp.* 60, 2207–2221. doi: 10.1002/lno.10196

Garratt, J. R. (1977). Review of drag coefficients over oceans and continents. *Month. Weather Rev.* 105, 915–929. doi: 10.1175/1520-0493

Gebhardt, S., Walter, S., Nausch, G., and Bange, H. W. (2004). Hydroxylamine (NH_2OH) in the Baltic Sea. *Biogeosci. Discus.* 1, 709–724. doi: 10.5194/bgd-1-709-2004

Gruber, N., and Sarmiento, J. L. (1997). Global patterns of marine nitrogen fixation and denitrification. *Global Biogeochem. Cycles* 11, 235–266. doi: 10.1029/97gb00077

Grundle, D. S., Maranger, R., and Juniper, S. K. (2012). Upper water column nitrous oxide distributions in the Northeast Subarctic Pacific Ocean. *Atmosphere-Ocean* 50, 475–486. doi: 10.1080/07055900.2012.727779

Hansen, H. P. (1999). "Determination of oxygen," in *Methods of Seawater Analysis*, eds K. Grasshoff, K. Kremling, and M. Ehrhardt (Hoboken: wiley), 75–89. doi: 10.1002/9783527613984.ch4

Hansen, H. P., and Koroleff, F. (1999). "Determination of nutrients," in *Methods of Seawater Analysis*, eds K. Grasshoff, K. Kremling, and M. Ehrhardt (Hoboken: wiley), 159–228. doi: 10.1002/9783527613984.ch10

Hu, A. Y., Yang, Z., Yu, C. P., and Jiao, N. Z. (2013). Dynamics of autotrophic marine planktonic thaumarchaeota in the East China Sea. *Plos One* 8:87. doi: 10.1371/journal.pone.0061087

Humbert, G., Sébilo, M., Fiat, J., Lang, L., Filali, A., Vaury, V., et al. (2020). Isotopic evidence for alteration of nitrous oxide emissions and producing pathways' contribution under nitrifying conditions. *Biogeosciences* 17, 979–993. doi: 10.5194/bg-17-979-2020

Jin, J., Liu, S. M., Ren, J. L., Liu, C. G., Zhang, J., Zhang, G. L., et al. (2013). Nutrient dynamics and coupling with phytoplankton species composition during the spring blooms in the Yellow Sea. *Deep Sea Res. Part II: Topical Stud. Oceanograp.* 97, 16–32. doi: 10.1016/j.dsr2.2013.05.002

Jurasinski, G., Janssen, M., Voss, M., Böttcher, M. E., Brede, M., Burchard, H., et al. (2018). Understanding the coastal ecocline: assessing sea–land interactions at non-tidal, low-lying coasts through interdisciplinary research. *Front. Marine Sci.* 5:342. doi: 10.3389/fmars.2018.00342

Kock, A., and Bange, H. W. (2013). Nitrite removal improves hydroxylamine analysis in aqueous solution by conversion with iron(III). *Environ. Chem.* 10:64. doi: 10.1071/en12141

Korth, F., Kock, A., Arevalo-Martinez, D. L., and Bange, H. W. (2019). Hydroxylamine as a potential indicator of nitrification in the open ocean. *Geophys. Res. Lett.* 46, 2158–2166. doi: 10.1029/2018GL080466

Kozlowski, J. A., Kits, K. D., and Stein, L. Y. (2016). Comparison of nitrogen oxide metabolism among diverse ammonia-oxidizing bacteria. *Front. Microbiol.* 7:1090. doi: 10.3389/fmicb.2016.01090

Kuypers, M. M. M., Marchant, H. K., and Kartal, B. (2018). The microbial nitrogen-cycling network. *Nature Rev. Microbiol.* 16, 263–276. doi: 10.1038/nrmicro.2018.9

Landolfi, A., Somes, C. J., Koeve, W., Zamora, L. M., and Oschlies, A. (2017). Oceanic nitrogen cycling and N_2O flux perturbations in the Anthropocene. *Global Biogeochem. Cycles* 31, 1236–1255. doi: 10.1002/2017gb005633

Laperriere, S. M., Nidzieko, N. J., Fox, R. J., Fisher, A. W., and Santoro, A. E. (2019). Observations of variable ammonia oxidation and nitrous oxide flux in a eutrophic estuary. *Estuaries Coasts* 42, 33–44. doi: 10.1007/s12237-018-0441-4

Lie, H.-J., and Cho, C.-H. (2016). Seasonal circulation patterns of the Yellow and East China Seas derived from satellite-tracked drifter trajectories and hydrographic observations. *Prog. Oceanograp.* 146, 121–141. doi: 10.1016/j.pocean.2016.06.004

Lin, X., Liu, M., Hou, L., Gao, D., Li, X., Lu, K., et al. (2017). Nitrogen losses in sediments of the East China Sea: spatiotemporal variations, controlling factors, and environmental implications. *J. Geophys. Res. Biogeosci.* 122, 2699–2715. doi: 10.1002/2017jg004036

Löscher, C. R., Kock, A., Könneke, M., LaRoche, J., Bange, H. W., and Schmitz, R. A. (2012). Production of oceanic nitrous oxide by ammonia-oxidizing archaea. *Biogeosciences* 9, 2419–2429. doi: 10.5194/bg-9-2419-2012

Ma, X., Bange, H. W., Eirund, G. K., and Arévalo-Martínez, D. L. (2020). Nitrous oxide and hydroxylamine measurements in the Southwest Indian Ocean. *J. Marine Syst.* 209:103062. doi: 10.1016/j.jmarsys.2018.03.003

Ma, X., Lennartz, S. T., and Bange, H. W. (2019). A multi-year observation of nitrous oxide at the Boknis Eck Time Series Station in the Eckernförde Bay (southwestern Baltic Sea). *Biogeosciences* 16, 4097–4111. doi: 10.5194/bg-16-4097-2019

Martens-Habbena, W., Berube, P. M., Urakawa, H., DelaTorre, J. R., and Stahl, D. A. (2009). Ammonia oxidation kinetics determine niche separation of nitrifying Archaea and Bacteria. *Nature* 461, 976–979. doi: 10.1038/nature08465

Martens-Habbena, W., Qin, W., Horak, R. E., Urakawa, H., Schauer, A. J., Moffett, J. W., et al. (2015). The production of nitric oxide by marine ammonia-oxidizing archaea and inhibition of archaeal ammonia oxidation by a nitric oxide scavenger. *Environ. Microbiol.* 17, 2261–2274. doi: 10.1111/1462-2920.12677

Nevison, C., Butler, J. H., and Elkins, J. W. (2003). Global distribution of N_2O and the ΔN_2O-AOU yield in the subsurface ocean. *Global Biogeochem. Cycles* 17:1119. doi: 10.1029/2003gb002068

Nightingale, P. D., Malin, G., Law, C. S., Watson, A. J., Liss, P. S., Liddicoat, M. I., et al. (2000). In situ evaluation of air-sea gas exchange parameterizations using novel conservative and volatile tracers. *Global Biogeochem. Cycles* 14, 373–387. doi: 10.1029/1999gb900091

Parsons, T. R., Maita, Y., and Lalli, C. M. (1984). "4.3 - Fluorometric Determination of Chlorophylls," in *A Manual of Chemical & Biological Methods for Seawater Analysis*, eds T. R. Parsons, Y. Maita, and C. M. Lalli (Amsterdam: Pergamon), 107–109.

Punshon, S., and Moore, R. M. (2004). Nitrous oxide production and consumption in a eutrophic coastal embayment. *Marine Chem.* 91, 37–51. doi: 10.1016/j.marchem.2004.04.003

Qin, W., Meinhardt, K. A., Moffett, J. W., Devol, A. H., Virginia Armbrust, E., Ingalls, A. E., et al. (2017). Influence of oxygen availability on the activities of ammonia-oxidizing archaea. *Environ. Microbiol. Rep.* 9, 250–256. doi: 10.1111/1758-2229.12525

Quan, Q., Mao, X., Yang, X., Hu, Y., Zhang, H., and Jiang, W. (2013). Seasonal variations of several main water masses in the southern Yellow Sea and East China Sea in 2011. *J. Ocean Univ. China* 12, 524–536. doi: 10.1007/s11802-013-2198-5

Santoro, A. E., Buchwald, C., McIlvin, M. R., and Casciotti, K. L. (2011). Isotopic signature of N_2O produced by marine ammonia-oxidizing archaea. *Science* 333, 1282–1285. doi: 10.1126/science.1208239

Schweiger, B., Hansen, H. P., and Bange, H. W. (2007). A time series of hydroxylamine (NH_2OH) in the southwestern Baltic Sea. *Geophys. Res. Lett.* 34, 86. doi: 10.1029/2007gl031086

Shen, F., Tang, R., Sun, X., and Liu, D. (2019). Simple methods for satellite identification of algal blooms and species using 10-year time series data from the East China Sea. *Remote Sens. Environ.* 235:111484. doi: 10.1016/j.rse.2019.111484

Stieglmeier, M., Mooshammer, M., Kitzler, B., Wanek, W., Zechmeister-Boltenstern, S., Richter, A., et al. (2014). Aerobic nitrous oxide production through N-nitrosating hybrid formation in ammonia-oxidizing archaea. *ISME J.* 8, 1135–1146. doi: 10.1038/ismej.2013.220

Stocker, T. F., Qin, D., Plattner, G.-K., Tignor, M. M. B., Allen, S. K., Boschung, J., et al. (2013). *Climate change 2013: the physical science basis: Working Group I contribution to the Fifth assessment report of the Intergovernmental Panel on Climate Change*. New York: Cambridge University Press.

Sutka, R. L., Ostrom, N. E., Ostrom, P. H., Gandhi, H., and Breznak, J. A. (2003). Nitrogen isotopomer site preference of N_2O produced by *Nitrosomonas europaea* and *Methylococcus capsulatus* Bath. *Rapid Commun. Mass Spectrom* 17, 738–745. doi: 10.1002/rcm.968

Tian, H., Xu, R., Canadell, J. G., Thompson, R. L., Winiwarter, W., Suntharalingam, P., et al. (2020). A comprehensive quantification of global nitrous oxide sources and sinks. *Nature* 586, 248–256. doi: 10.1038/s41586-020-2780-0

Toyoda, S., Yoshida, O., Yamagishi, H., Fujii, A., Yoshida, N., and Watanabe, S. (2019). Identifying the origin of nitrous oxide dissolved in deep ocean by concentration and isotopocule analyses. *Sci. Rep.* 9:7790. doi: 10.1038/s41598-019-44224-0

Trimmer, M., Chronopoulou, P. M., Maanoja, S. T., Upstill-Goddard, R. C., Kitidis, V., and Purdy, K. J. (2016). Nitrous oxide as a function of oxygen and archaeal gene abundance in the North Pacific. *Nature Commun.* 7:13451. doi: 10.1038/ncomms13451

Tseng, H.-C., Chen, C.-T. A., Borges, A. V., DelValls, T. A., Lai, C.-M., and Chen, T.-Y. (2016). Distributions and sea-to-air fluxes of nitrous oxide in the South China Sea and the West Philippines Sea. *Deep Sea Res. Part I: Oceanograp. Res. Papers* 115, 131–144. doi: 10.1016/j.dsr.2016.06.006

Vajrala, N., Martens-Habbena, W., Sayavedra-Soto, L. A., Schauer, A., Bottomley, P. J., Stahl, D. A., et al. (2013). Hydroxylamine as an intermediate in ammonia oxidation by globally abundant marine archaea. *Proc. Nat. Acad. Sci. USA* 110, 1006–1011. doi: 10.1073/pnas.1214272110

Von Breymann, M. T., De Angelis, M. A., and Gordon, L. I. (1982). Gas chromatography with electron capture detection for determination of hydroxylamine in seawater. *Anal. Chem.* 54, 1209–1210. doi: 10.1021/ac00244a048

Walker, C. B., DelaTorre, J. R., Klotz, M. G., Urakawa, H., Pinel, N., Arp, D. J., et al. (2010). Nitrosopumilus maritimus genome reveals unique mechanisms for nitrification and autotrophy in globally distributed marine crenarchaea. *Proc. Nat. Acad. Sci. USA* 107, 8818–8823. doi: 10.1073/pnas.0913533107

Wang, J., Yan, W., Chen, N., Li, X., and Liu, L. (2015). Modeled long-term changes of DIN:DIP ratio in the Changjiang River in relation to Chl-α and DO concentrations in adjacent estuary. *Estuarine Coast. Shelf Sci.* 166, 153–160. doi: 10.1016/j.ecss.2014.11.028

Wang, L., Zhang, G., Zhu, Z., Li, J., Liu, S., Ye, W., et al. (2016). Distribution and sea-to-air flux of nitrous oxide in the East China Sea during the summer of 2013. *Contin. Shelf Res.* 123, 99–110. doi: 10.1016/j.csr.2016.05.001

Wanninkhof, R. (1992). Relationship between wind speed and gas exchange over the ocean. *J. Geophys. Res.* 97:7373. doi: 10.1029/92jc00188

Wanninkhof, R. (2014). Relationship between wind speed and gas exchange over the ocean revisited. *Limnol. Oceanograp. Methods* 12, 351–362. doi: 10.4319/lom.2014.12.351

Weiss, R. F., and Price, B. A. (1980). Nitrous oxide solubility in water and seawater. *Marine Chem.* 8, 347–359. doi: 10.1016/0304-4203(80)90024-9

Wilson, S. T., Al-Haj, A. N., Bourbonnais, A., Frey, C., Fulweiler, R. W., Kessler, J. D., et al. (2020). Ideas and perspectives: a strategic assessment of methane and nitrous oxide measurements in the marine environment. *Biogeosciences* 17, 5809–5828. doi: 10.5194/bg-17-5809-2020

Wilson, S. T., Bange, H. W., Arévalo-Martínez, D. L., Barnes, J., Borges, A. V., Brown, I., et al. (2018). An intercomparison of oceanic methane and nitrous oxide measurements. *Biogeosciences* 15, 5891–5907. doi: 10.5194/bg-15-5891-2018

Wilson, S. T., del Valle, D. A., Segura-Noguera, M., and Karl, D. M. (2014). A role for nitrite in the production of nitrous oxide in the lower euphotic zone of the oligotrophic North Pacific Ocean. *Deep Sea Res. Part I: Oceanograp. Res. Papers* 85, 47–55. doi: 10.1016/j.dsr.2013.11.008

Yang, J., Zhang, G., Zheng, L., and Zhang, F. (2009). Seasonal variations of fluxes and distributions of dissolved N_2O in the North Yellow Sea. *Environ. Sci.* 30, 656–662.

Yang, S., Chang, B. X., Warner, M. J., Weber, T. S., Bourbonnais, A. M., Santoro, A. E., et al. (2020). Global reconstruction reduces the uncertainty of oceanic nitrous oxide emissions and reveals a vigorous seasonal cycle. *Proc. Nat. Acad. Sci. USA* 117, 11954–11960. doi: 10.1073/pnas.1921914117

Zeng, Y., Li, H., and Jiao, N. (2007). Phylogenetic diversity of planktonic archaea in the estuarine region of East China Sea. *Microbiol. Res.* 162, 26–36. doi: 10.1016/j.micres.2006.03.007

Zhang, G., Zhang, J., Ren, J., Li, J., and Liu, S. (2008). Distributions and sea-to-air fluxes of methane and nitrous oxide in the North East China Sea in summer. *Marine Chem.* 110, 42–55. doi: 10.1016/j.marchem.2008.02.005

Zhang, G.-L., Liu, S.-M., Casciotti, K. L., Forbes, M. S., Gu, X.-J., Ren, Y.-Y., et al. (2019). Distribution of concentration and stable isotopic composition of N_2O in the shelf and slope of the northern South China Sea: implications for production and emission. *J. Geophys. Res.: Oceans* 124, 6218–6234. doi: 10.1029/2019JC014947

Zhang, G. L., Zhang, J., Liu, S. M., Ren, J. L., and Zhao, Y. C. (2010). Nitrous oxide in the Changjiang (Yangtze River) Estuary and its adjacent marine area: Riverine input, sediment release and atmospheric fluxes. *Biogeosciences* 7, 3505–3516. doi: 10.5194/bg-7-3505-2010

Zhao, Y., Zhao, L., Zhang, W., Sun, J., Huang, L., Li, J., et al. (2016). Variations of picoplankton abundances during blooms in the East China Sea. *Deep Sea Res. Part II: Topical Stud. Oceanograp.* 124, 100–108. doi: 10.1016/j.dsr2.2015.03.010

Zhou, P., Song, X., Yuan, Y., Wang, W., Chi, L., Cao, X., et al. (2018). Intrusion of the Kuroshio subsurface water in the southern East China Sea and its variation in 2014 and 2015 traced by dissolved inorganic iodine species. *Prog. Oceanograp.* 165, 287–298. doi: 10.1016/j.pocean.2018.06.011

Conflict of Interest: The authors declare that the research was conducted in the absence of any commercial or financial relationships that could be construed as a potential conflict of interest.

Publisher's Note: All claims expressed in this article are solely those of the authors and do not necessarily represent those of their affiliated organizations, or those of the publisher, the editors and the reviewers. Any product that may be evaluated in this article, or claim that may be made by its manufacturer, is not guaranteed or endorsed by the publisher.